Article

X-ray Absorption Spectroscopy Studies of a Molecular CO$_2$-Reduction Catalyst Deposited on Graphitic Carbon Nitride

Junying Li, Peipei Huang, Facheng Guo, Jiahao Huang, Shuting Xiang, Ke Yang, N. Aaron Deskins, Victor S. Batista, Gonghu Li,* and Anatoly I. Frenkel*

Read Online

ACCESS | Metrics & More | Article Recommendations | Supporting Information

ABSTRACT: Metal−ligand complexes have been extensively explored as well-defined molecular catalysts in small molecule activation reactions such as carbon dioxide (CO$_2$) reduction. Many hybrid photocatalysts have been prepared by coupling such complexes with photoactive surfaces for use in solar CO$_2$ reduction. In this work, we employ X-ray absorption near edge structure (XANES) and extended X-ray absorption fine structure (EXAFS) spectroscopies, density functional theory (DFT) and computational XANES modeling to interrogate the structure of a hybrid photocatalyst consisting of a macrocyclic cobalt complex deposited on graphitic carbon nitride (C$_3$N$_4$). Results show that the cobalt complex binds on C$_3$N$_4$ through surface OH or NH$_2$ groups. By refining the local geometry and binding sites of this well-defined molecular cobalt complex on C$_3$N$_4$, we established an important benchmark for modeling a large class of molecular catalysts that can be adapted to in situ/operando studies and further enhanced by applying chemometrics-based approaches and machine learning methods of XANES data analysis.
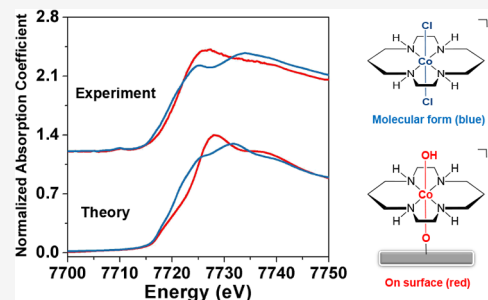
1. INTRODUCTION

The rising concentration of atmospheric carbon dioxide (CO$_2$) is thought to be responsible for ocean acidification and other climate changes, such as global warming, sea-level rise, and extreme weather conditions.[1−3] The elevated CO$_2$ level and gradual depletion of fossil fuels have stimulated the development of methods to address the energy crisis and solve environmental problems faced by the whole world.[4] Solar-driven CO$_2$ reduction is among the most promising approaches to utilize renewable energy to convert CO$_2$ to valuable chemicals and fuels while mitigating the increasing CO$_2$ concentration in the atmosphere.[5−8] Currently known photocatalysts for CO$_2$ reduction include molecular and supramolecular complexes as well as inorganic semiconductors.[9−14]

In recent years, hybrid photocatalysts consisting of well-defined molecular complexes grafted on semiconductor photosensitizers have attracted strong interest for use in solar CO$_2$ reduction.[15−21] For example, Kuriki et al.[22] fabricated several high-performance hybrid photocatalytic systems with ruthenium complexes on graphitic carbon nitride (C$_3$N$_4$) for photocatalytic CO$_2$ reduction. The ruthenium complexes were derivatized with different functional groups (−H, −COOH, −PO$_3$H$_2$, and −CH$_2$PO$_3$H$_2$) for immobilization on surfaces. However, the explicit binding interactions between the metal complexes and light-absorbing semiconductors were not clearly discussed. In solar fuel research, more catalysts based on earth-abundant metals have recently been reported.[23] In particular, there are many studies using cobalt (Co)-based molecular

catalysts because of their outstanding performance, low cost, and stability.[24−28] Reisner and co-workers[23,29] deposited Co phthalocyanine cyanine on mesoporous carbon nitride with the help of a week $\pi-\pi$ stacking interaction and obtained a turnover number of 90 for CO$_2$ conversion to CO after 60 h under UV/vis light. In the recent work by Wang and co-workers,[30] a Co phthalocyanine complex containing −COOH groups was deposited on C$_3$N$_4$ for photocatalytic CO$_2$ reduction. The −COOH groups enabled high surface coverage of the Co complex and promoted its catalytic property. Robert and co-workers[31] attached a Co-quaterpyridine molecular complex onto carbon nitride through an amide linkage, which showed a remarkable selectivity (98%) for CO production under visible light.

Our recent studies have focused on using [Co(cyclam)Cl$_2$]-Cl, where cyclam is 1,4,8,11-tetraazacyclotetradecane, as the molecular catalyst for solar CO$_2$ reduction. Selective CO$_2$-to-CO conversion has been achieved using [Co(cyclam)Cl$_2$]Cl with *p*-terphenyl as a photosensitizer under UV light irradiation,[32] as shown in Scheme 1a. In our previous work,[33−36] [Co(cyclam)Cl$_2$]Cl was deposited on the surfaces of TiO$_2$ and C$_3$N$_4$ for use in photocatalytic CO$_2$ reduction. In
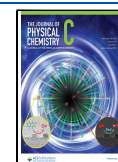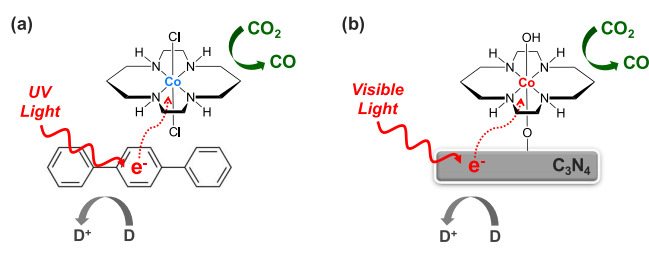
Scheme 1. Schematic of CO_2 Reduction on a Macrocyclic Cobalt Catalyst Using (a) *p*-Terphenyl and (b) C_3N_4 as the Photosensitizers. D is an Electron Donor.

this current study, we focus on structural investigation of $[Co(cyclam)Cl_2]Cl$ deposited on C_3N_4, which is denoted "CoX/C_3N_4" since the axial ligands on the Co center are different from the molecular complex upon surface deposition. As will be discussed, the Cl ligands in $[Co(cyclam)Cl_2]Cl$ could be replaced with −OH groups (Scheme 1b) during the synthesis of CoX/C_3N_4 in the presence of a weak base, triethylamine (TEA).

C_3N_4 is an interesting material that has been extensively studied in photocatalysis due to its low cost, high thermal and chemical stability, nitrogen-rich structure, and suitable bandgap.[25,37,38] In photocatalytic CO_2 reduction, triethanolamine (TEOA) is often used as a sacrificial electron donor[10] for C_3N_4-based materials. Recently, we prepared single atom catalysts by coordinating single Co^{2+} sites on C_3N_4, in the absence of additional ligands, via a simple microwave method.[37,39,40] Selective CO_2 reduction under visible-light irradiation was achieved by using such single Co^{2+} sites. However, the single Co^{2+} sites only exist at low cobalt loadings on C_3N_4; at high loadings, catalytically inactive CoO_x formed instead of the single Co^{2+} sites. Even at low cobalt loadings, different single Co^{2+} sites might co-exist.[40]

This current study focuses on the structural investigation of CoX/C_3N_4 prepared by depositing $[Co(cyclam)Cl_2]Cl$ on C_3N_4. Due to the well-defined structure of $[Co(cyclam)Cl_2]Cl$, all the cobalt sites in CoX/C_3N_4 are identical. Furthermore, the use of C_3N_4 as the solid-state photosensitizer enables CO_2 reduction under visible-light irradiation (Scheme 1b).

To obtain atomic-level structural information, we previously employed X-ray absorption spectroscopy (XAS) to characterize transition metal catalysts in both ex-situ and in-situ/operando studies.[25,41−45] Specifically, the extended X-ray absorption fine structure (EXAFS) analysis can provide valuable insights into the local geometric structure and coordination environment of the metal sites.[46−48] The X-ray absorption near edge structure (XANES) spectra are particularly sensitive to the electronic structure of the metal center and its local environment.[49−52] Our recent work[36] utilized XANES spectra of CoX/C_3N_4 to probe possible intermediates during photocatalytic CO_2 reduction. While the chemometrics-based approach for separating between different Co structures coexisting in reaction conditions was successful, the choice of the structural model for using a machine learning − based method of XANES data analysis was guided by human expertise only. To address this and other challenges in studying the catalyst structure and local environment, new data analysis protocols need to be developed.[53] In terms of the XANES analysis of atomically dispersed catalysts, one important challenge is the lack of knowledge of multiple possible structures for theoretical XANES modeling. As an important

step towards solving this general speciation problem, in this study, we combine theoretical XANES modeling with density functional theory (DFT) simulations and EXAFS data analysis to further understand the local structure of Co in a well-defined, supported molecular catalyst with demonstrated activity in photocatalytic CO_2 reduction.

2. EXPERIMENTAL

2.1. Materials. Acetonitrile (99.999%) and 1,4,8,11-tetraazacyclotetradecane (cyclam, 98%) were obtained from Sigma-Aldrich. Methanol and chloroform (99.8%) were purchased from Pharmco-Aaper. Triethylamine (TEA, ≥99%) was obtained from Acros. Triethanolamine (TEOA, ≥99%) and urea (98%) were obtained from Alfa Aesar. All reagents were used without further purification.

2.2. Synthesis of C_3N_4. Graphitic carbon nitride (C_3N_4) was prepared by pyrolysis of urea. In a typical synthesis, 20 g urea was put into a covered crucible and calcined in a muffle furnace at 600 °C for 4 h (ramp rate 5 °C/min). Note: pyrolysis of this urea sample (98% purity) produced a C-doped C_3N_4 sample. The quality of C-doped C_3N_4 may vary due to differences in the composition of commercial urea samples at this purity level. We have reported an improved method to synthesize C-doped C_3N_4 using urea of the highest purity (99.5+%) and dextrose as the source of C dopant.[37]

2.3. Catalyst Synthesis. The molecular catalyst, $[Co(cyclam)Cl_2]Cl$, was synthesized following an established method. To deposit $[Co(cyclam)Cl_2]Cl$ on C_3N_4, 100 mg C_3N_4 were mixed with a specific amount of $[Co(cyclam)Cl_2]Cl$ in 7.5 mL acetonitrile. Then 65 μL TEA was added to the mixture, which was subsequently stirred for 2 h. The mixture in a capped reaction vessel was placed in a CEM Discover single-mode microwave reactor and was heated to 80 °C for 120 min. After the microwave reaction, the resulting precipitate was recovered by centrifugation and washed twice with chloroform, methanol, and acetonitrile, respectively. After drying at room temperature, a photocatalyst, denoted "CoX/C_3N_4", was obtained.

2.4. Materials Characterization. Elemental analysis was conducted by acid digestion, followed by quantification using a Varian Vista AX induced coupled plasma atomic emission spectrometer (ICP-AES). X-ray diffraction (XRD) patterns of powder samples were collected on a Rigaku X.D.S. 2000 diffractometer using nickel-filtered Cu Kα radiation (λ = 1.5418 Å). Scanning electron microscopy (SEM) images were collected on an Amray 3300FE field emission SEM with P.G.T. Imix-PC microanalysis system. Ultraviolet-visible (UV−Vis) spectra were obtained on a Cary 50 Bio spectrophotometer. A Barrelino diffuse reflectance probe was used to collect UV−Vis spectra of powder samples using $BaSO_4$ as a standard. Fourier transform infrared (FTIR) spectra were collected on a Thermo Nicolet iS10 FTIR spectrometer.

2.5. Photocatalytic Testing. In photocatalytic CO_2 reduction, a specific amount (1.0 mg) of catalyst was dispersed in a 4.0 mL acetonitrile solution containing TEOA (acetonitrile: TEOA = 4:1 v/v) in a quartz test tube (Scheme S1). In the testing using a physical mixture of $[Co(cyclam)Cl_2]Cl$ and C_3N_4, the reaction solution contained 13 μL methanol for dissolving $[Co(cyclam)Cl_2]Cl$. Prior to photocatalytic testing, the reaction solution was bubbled with CO_2 (99.999%, Airgas) in the dark for 20 min. The reaction solution was then irradiated with a halogen lamp equipped with a water filter. Light intensity on the reaction solution was

fixed at 200 mW/cm^2. The head space above the reaction solution was sampled with a gas-tight syringe at different time intervals for product analysis using an Agilent 7820 GC equipped with a thermal conductivity detector. detector and a 60/80 Carboxen-1000 packed column (Supelco).

2.6. X-ray Absorption Spectroscopy. X-ray absorption spectra at Co K-edge were taken at the beamline 7-BM (QAS) of NSLS-II at Brookhaven National Laboratory. An Si (111) double crystal monochromator was used. CoX/C$_3$N$_4$ was measured in fluorescence mode. The raw XAFS spectra were analyzed utilizing the Athena and Artemis interfaces of the Demeter software package.[54] Theoretical XANES spectra were calculated using FEFF code (version 9.6.4).[55] The input parameters are provided in the SI.

2.7. Computational Modeling. The Vienna Ab initio Simulation Package[56–59] (VASP) version 5.4.1 was used for all Density Functional Theory (DFT) calculations. The electron-ion interactions were described by the Perdew–Burke–Ernerhof[60] (PBE) exchange-correlation function with the projected augmented-wave method[61,62] (PAW). The DFT-D3 method[63] with Becke–Jonson damping[64] was used to consider the van der Waals interactions. The cut-off energy of the plane wave basis was chosen to be 700 eV. The energy convergence criterion was set to be 10^{-6} eV per unit cell. The Gaussian smearing with $\sigma = 0.1$ eV was used for all calculations and the maximum optimization step-size was at 0.4 Bohr. A 1 × 1 × 1 Monkhorst–Pack type k-point grid[65] was used to sample the Brillouin zone during the geometry optimization.

3. RESULTS AND DISCUSSION

The hybrid photocatalyst in this study, CoX/C$_3$N$_4$, was prepared following a microwave method as described in the experimental section. A weak base, TEA, was used to facilitate the binding of [Co(cyclam)Cl$_2$]Cl on C$_3$N$_4$ (Figure S1 in the Supplementary Information). A negligible amount of [Co(cyclam)Cl$_2$]Cl was deposited on C$_3$N$_4$ in the absence of TEA. In this present study, we focus on a CoX/C$_3$N$_4$ sample with a loading of 0.018 μmol cobalt per 1 mg C$_3$N$_4$. At this level of cobalt loadings, the presence of [Co(cyclam)Cl$_2$]Cl on C$_3$N$_4$ was not seen using X-ray powder diffraction (Figure S2), UV–Vis (Figure S3), infrared spectroscopy (Figure S4), or microscopy (Figure S5). Instead, XAS appeared to be a highly sensitive technique to confirm the presence of cobalt in CoX/C$_3$N$_4$, as will be discussed later.

The synthesized CoX/C$_3$N$_4$ was evaluated in photocatalytic CO$_2$ reduction using TEOA as a sacrificial electron donor. A halogen lamp was used as the light source to provide photons with wavelengths in the range of 350−800 nm (Figure S6). Under the experimental conditions employed in this study, CO and H$_2$ were detected by gas chromatography as the major products. Turnover numbers (TONs) were calculated by taking the ratio between the amounts of products and the amount of Co present in the reaction suspension. After photocatalysis for 2 h, TONs of 47 and 17 were obtained for CO and H$_2$, respectively, representing a selectivity of 74% towards CO production. A TON of more than 160 for CO production was obtained after photocatalysis for an extended period using CoX/C$_3$N$_4$ under visible-light irradiation ($\lambda >$ 420 nm, Figure S7). Furthermore, the synthesized CoX/C$_3$N$_4$ demonstrated reasonable recyclability in photocatalysis (Figure S8). Under the same conditions, no CO was produced using a physical mixture of [Co(cyclam)Cl$_2$]Cl and C$_3$N$_4$ (Figure 1) or using bare C$_3$N$_4$.
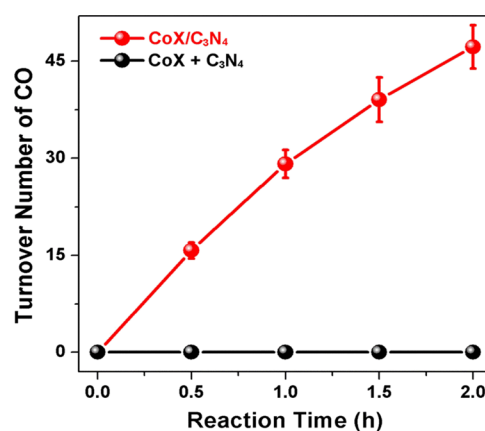

Figure 1. CO production in photocatalytic CO$_2$ reduction using 1.0 mg CoX/C$_3$N$_4$ (red), prepared by the microwave method, and the simple mixture of 1 mg C$_3$N$_4$ and [Co(cyclam)Cl$_2$]Cl (black). In both tests, the amount of [Co(cyclam)Cl$_2$]Cl was 0.018 μmol.

The results shown in Figure 1 clearly indicate the key role of attaching [Co(cyclam)Cl$_2$]Cl on C$_3$N$_4$ in enabling photocatalysis using CoX/C$_3$N$_4$. In order to obtain detailed structural information on such surface attachment, CoX/C$_3$N$_4$ in the powder form was investigated using XANES and EXAFS. Figure 2 shows the Co K-edge XANES spectrum of
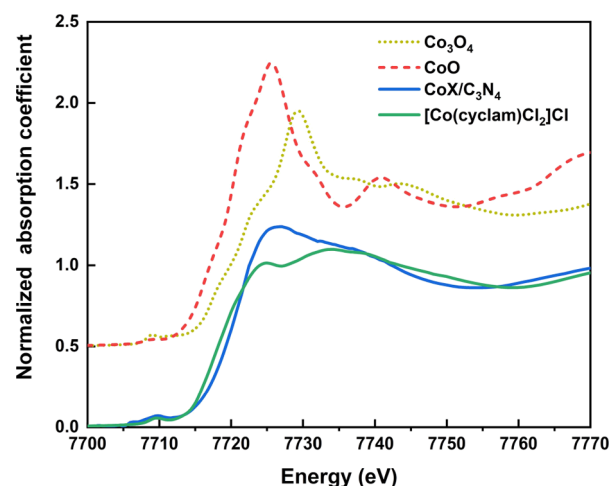

Figure 2. Normalized Co K-edge XANES spectra of [Co(cyclam)Cl$_2$]Cl (green), CoX/C$_3$N$_4$ (blue), and two Co oxide samples as references.

CoX/C$_3$N$_4$, which has different features from that of [Co(cyclam)Cl$_2$]Cl. Such differences suggest that the coordination environment of cobalt significantly changed upon depositing [Co(cyclam)Cl$_2$]Cl on C$_3$N$_4$. Based on prior studies,[33–36] we hypothesize that the two axial Cl ligands of [Co(cyclam)Cl$_2$]Cl were replaced with one OH group and one surface −O− or −NH− group upon deposition on C$_3$N$_4$ through the microwave synthesis in the presence of TEA. In the following context, we combine theoretical XANES modeling with DFT simulations and EXAFS data analysis to test our hypothesis.

In the proposed structure of CoX/C$_3$N$_4$, the "CoX" unit differs from [Co(cyclam)Cl$_2$]Cl in that it contains a hydroxyl group instead of the Cl ligand. In addition, the CoX/C$_3$N$_4$ complex poses a strong challenge to the task of XANES

modeling because of the lack of knowledge about specific binding sites and local geometry. DFT simulations were performed to obtain possible structures of CoX anchored on C_3N_4, which is known to contain surface NH_2 and OH groups. Other surface functional groups on C_3N_4, such as secondary amine groups, were also considered as potential binding sites in our DFT simulations but attempts to obtain stable structures on such sites failed. Therefore, the anchoring of CoX to C_3N_4 through either a surface $-NH-$ or $-O-$ group represents the most probable modes, and their optimized structures are shown in Figures 3 and 4, respectively. The
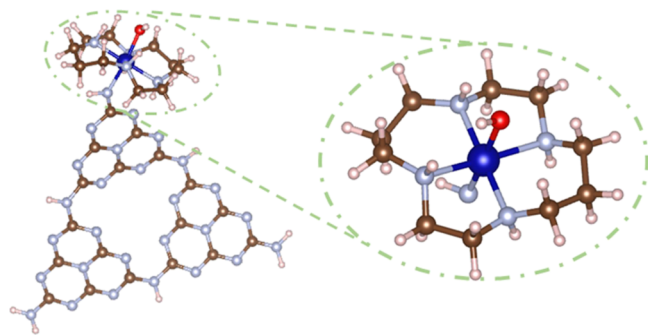
Figure 3. DFT optimized structure of CoX attached to C_3N_4 through a nitrogen atom. Color scheme: Co (blue), N (silver), C (brown), O (red), and H (pink).
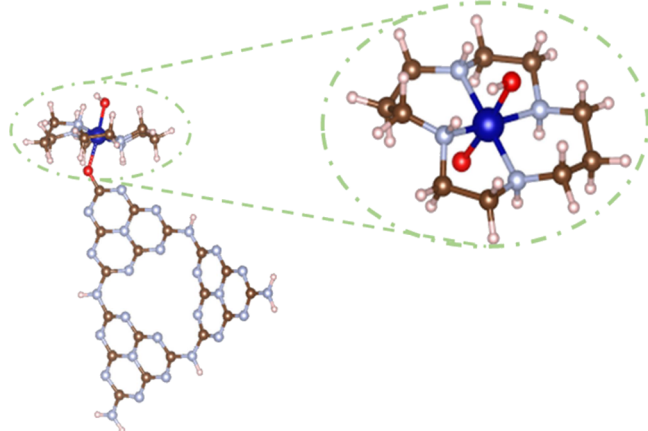

Figure 4. DFT optimized structure of CoX attached to C_3N_4 through an oxygen atom. Color scheme: Co (blue), N (silver), C (brown), O (red), and H (pink).

optimized structures shown in Figures 3 and 4 have similar energies and distances between the Co center of CoX and C_3N_4. In particular, the Co–N (N on C_3N_4) bond length in the structure shown in Figure 3 is predicted to be 1.96 Å, while the Co–O (O on C_3N_4) bond length in the structure shown in Figure 4 is calculated to be 2.00 Å.

After obtaining the DFT-optimized structural coordinates (see the output files in the VASP format in the Supplementary Information), we used them as a basis for theoretical XANES modeling. In such theoretical studies, the experimental XANES spectrum of $[Co(cyclam)Cl_2]Cl$ was chosen as a standard to optimize the FEFF parameters for simulating the spectra of CoX on C_3N_4. Both the experimental and theoretical XANES spectra of $[Co(cyclam)Cl_2]Cl$ are shown in Figure 5. As can be seen from Figure 5, the theoretical spectrum of $[Co(cyclam)-$

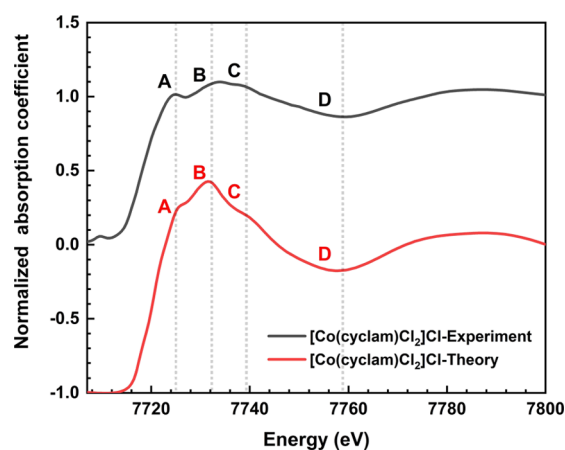$Cl_2]Cl$ contains all four key features (A, B, C, and D) of the experimental spectrum.

Figure 5. Experimental and simulated XANES spectra of Co atoms in $[Co(cyclam)Cl_2]Cl$.

Theoretical XANES spectra of the DFT − optimized structures shown in Figures 3 and 4 were then calculated and the results are shown in Figure 6. A strong difference
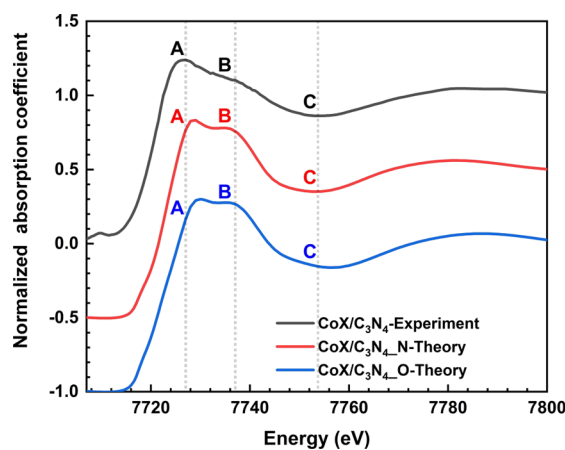

Figure 6. Experimental XANES spectrum of CoX/C_3N_4 (top), and simulated XANES spectra of CoX using DFT optimized structures shown in Figure 3 (middle) and Figure 4 (bottom).

between the experimental data for $[Co(cyclam)Cl_2]Cl$ and CoX/C_3N_4 (Figure 2) is captured by the difference between their corresponding theoretical spectra (Figures 5 and 6). As can be seen from Figure 6, both simulated XANES spectra are in good qualitative agreement with the experimental XANES spectrum of CoX/C_3N_4. However, it remains unclear whether CoX is attached to C_3N_4 through a nitrogen or oxygen atom, based on the results shown in Figure 6.

We further analyzed EXAFS spectra to gain quantitative information on the structure of CoX/C_3N_4 and correlate with the predictions by DFT-XANES analyses. Figure 7 shows the Co K-edge EXAFS spectra of $[Co(cyclam)Cl_2]Cl$ and CoX/C_3N_4 in r-space. Both spectra display characteristics associated with single cobalt sites, compared with those of cobalt oxides. In the spectrum of $[Co(cyclam)Cl_2]Cl$, the first peak is seen at ca. 1.55 Å (uncorrected for the photoelectron phase shift). In contrast, the first peak is around 1.35 Å in the spectrum of CoX/C_3N_4. This shift upon surface deposition can be
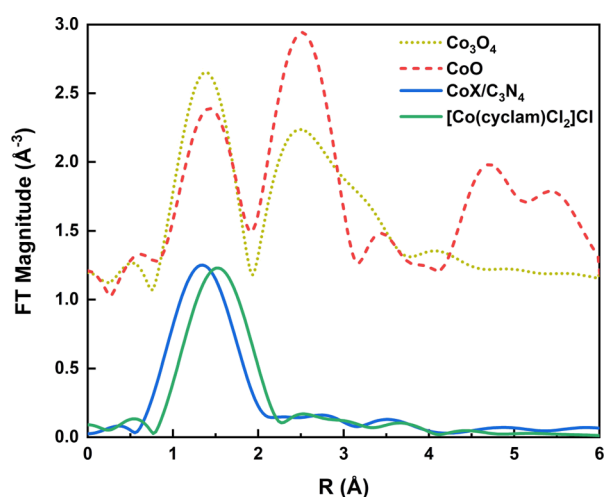
Figure 7. Fourier transform magnitudes of k^2-weighted Co K-edge EXAFS spectra of $[Co(cyclam)Cl_2]Cl$ (green), CoX/C$_3$N$_4$ (blue), and two Co oxides. The k-range from 2 to 7 Å^{-1} and k^2 weighting were used in the Fourier transform.

explained by our proposed structures shown in Figures 3 and 4. Specifically, the peak in the spectrum of CoX/C$_3$N$_4$ corresponds to Co−N (bond length ∼ 1.98 Å) and Co−O (bond length ∼ 1.92 Å) contributions from the first shell.[66] The peak in the spectrum of $[Co(cyclam)Cl_2]Cl$ between 1 and 2 Å (uncorrected for the photoelectron phase shift) is contributed by the Co−Cl (bond length ∼ 2.25 Å) and Co−N (bond length ∼ 1.98 Å) pairs.

Therefore, the difference in the spectra of $[Co(cyclam)Cl_2]Cl$ and CoX/C$_3$N$_4$ shown in Figure 7 originated from the replacement of Cl ligands with N/O-containing ligands upon depositing $[Co(cyclam)Cl_2]Cl$ on C$_3$N$_4$.

The EXAFS spectra were analyzed by conventional Levenberg−Marquardt nonlinear least squares method, in which FEFF6 theory was fit to the experimental data while varying adjustable parameters, such as coordination numbers, bond lengths and their variances. The Co foil measured at the same beamline was first analyzed to obtain the passive electron reduction factor S_0^2 (0.61), which is used to fitting the spectra of all samples. Table 1 summarizes fitting parameters obtained for the EXAFS analysis of $[Co(cyclam)Cl_2]Cl$ and CoX/C$_3$N$_4$ (Figure 8). For $[Co(cyclam)Cl_2]Cl$, the Co−Cl and Co−N scattering paths were chosen to fit the first peak. The resulting coordination numbers corresponding to Co−N and Co−Cl bonds are 3.5 ± 1.2 and 2.0 ± 1.2, respectively. The Co−N and Co−Cl bond lengths were obtained to be 1.94 ± 0.04 Å and 2.25 ± 0.04 Å, respectively, in excellent agreement with previously published results for a similar macrocyclic cobalt compound.[67] The Co−O scattering path was chosen to fit the first peak of CoX/C$_3$N$_4$ for the quantitative EXAFS data analysis. The coordination number of Co−O nearest neighbors was found to be 6.3 ± 1.4.

In this study, results from theoretical XANES modeling and EXAFS data analysis strongly support the DFT optimized structures (Figures 3 and 4). Therefore, Co binding to C$_3$N$_4$ via surface N/O atoms represents a plausible model describing the anchoring of CoX on C$_3$N$_4$, even though our results were not able to distinguish between contributions from N and O atoms. As mentioned earlier, attaching CoX to the light-absorbing C$_3$N$_4$ is critical to the CO$_2$-reduction activity demonstrated by CoX/C$_3$N$_4$ (Figure 1).

It is worth noting that CoX/C$_3$N$_4$ likely underwent some structural changes under the photocatalytic conditions employed in this study, despite its demonstrated recyclability (Figure S8). Figures S9 and S10 show the XAS spectra of CoX/C$_3$N$_4$ before and after photocatalysis. Some minor differences are seen in the comparison between the spectra. While it is difficult to say what exactly happened to CoX upon photocatalysis, it is clear that there is no evidence of Co reducing (Figure S9) or aggregation (Figure S10). Our future work includes detailed mechanistic studies of light-induced electron transfer and photostability of CoX/C$_3$N$_4$ using time-resolved techniques, as well as coupling other Co-based molecular catalysts[68] with C$_3$N$_4$ for photocatalysis.

4. CONCLUSIONS

In summary, we have synthesized a hybrid photocatalyst by depositing a macrocyclic cobalt complex on light-absorbing C$_3$N$_4$. We combined theoretical XANES modeling with DFT simulations and EXAFS data analysis to probe the structure of the hybrid photocatalyst. Our results indicate that surface attachment of the cobalt complex likely occurs by replacing two axial Cl ligands with one OH group and one surface NH or O group during the synthesis in the presence of a weak base. Our study provides molecular level insights into the structures of this type of hybrid photocatalyst consisting of metal−ligand complexes on heterogeneous surfaces.

One key result of our work is a new XANES data analysis protocol that relies on the application of DFT for selecting candidate structures for Co K-edge XANES modeling for the hybrid photocatalyst bound to the support. The lack of knowledge of the geometry of the catalyst-support sites hampers such studies in which atomically dispersed catalysts of size-selective clusters are analyzed by "inverting" their XANES spectra. This method opens a new opportunity for structural analysis of such photocatalysts using a machine learning approach.[69,70] Namely, multiple spectra calculated theoretically may be used for training a neural network classifier, similar to an analogous approach developed recently for predicting new topological insulators.[71] Such a classifier will be used for interpreting the spectra of different hybrid photocatalysts in terms of different classes of local structure and local geometry of the support, for subsequent structural refinement. In comparison, current efforts are mostly limited to chemometrics-based approaches and require a large number of experimental spectra for such a classification.[36,70]

Table 1. Fitting Parameters for $[Co(Cyclam)Cl_2]Cl$ and CoX/C$_3$N$_4$: The Neighboring Pairs, their Coordination Numbers, Distances and Mean Square Relative Displacements, and the Correction to the Photoelectron Energy Origin

samples	paths	coordination number	R (Å)	σ² (Å²)	ΔE (eV)
$[Co(cyclam)Cl_2]Cl$	Co−N	3.5 ± 1.2	1.94 ± 0.04	0.000 ± 0.007	1 ± 4
	Co−Cl	2.0 ± 1.2	2.25 ± 0.04	0.000 ± 0.007	1 ± 4
CoX/C$_3$N$_4$	Co−O	6.3 ± 1.4	1.91 ± 0.02	0.009 ± 0.005	1 ± 4

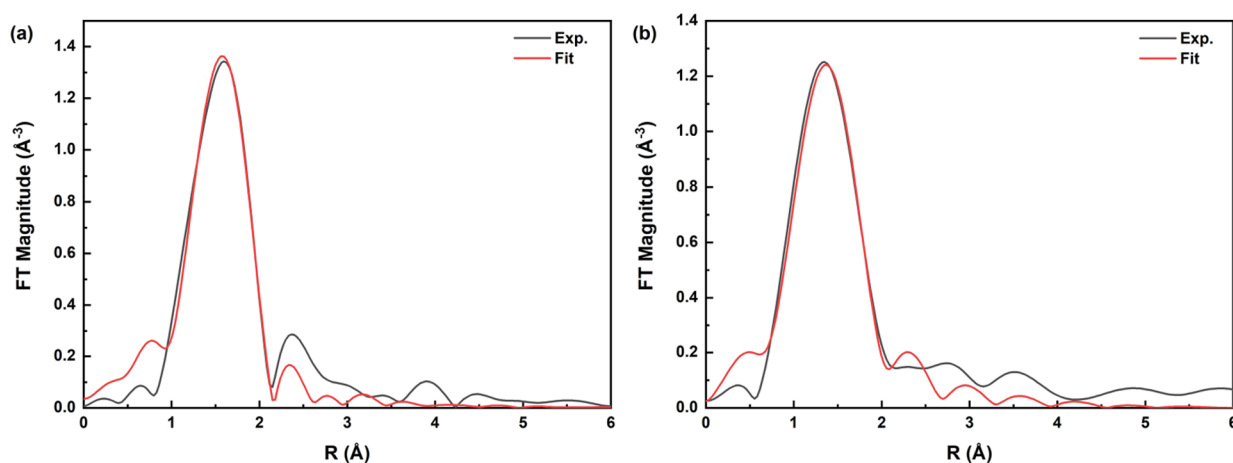**Figure 8.** Fourier transform magnitudes of k^2-weighted Co K-edge EXAFS spectra of (a) $[Co(cyclam)Cl_2]Cl$ and (b) CoX/C_3N_4 and their theoretical fits. The k-range is from 2 to 7 Å^{-1}. The r-ranges used for fitting the data for $[Co(cyclam)Cl_2]Cl$ and CoX/C_3N_4 were 1.1−2.8 Å and 1.1−2.6 Å, respectively.

■ ASSOCIATED CONTENT

Ⓢ Supporting Information

The Supporting Information is available free of charge at https://pubs.acs.org/doi/10.1021/acs.jpcc.2c08587.

> Supplementary figures of additional characterization data, DFT-optimized structural coordinates, and input parameters for XANES simulation (PDF).

■ AUTHOR INFORMATION

Corresponding Authors

Gonghu Li − *Department of Chemistry, University of New Hampshire, Durham, New Hampshire 03857, United States;* ⓞ orcid.org/0000-0002-2924-3597; Email: gonghu.li@unh.edu

Anatoly I. Frenkel − *Department of Materials Science and Chemical Engineering, Stony Brook University, Stony Brook, New York 11794, United States; Division of Chemistry, Brookhaven National Laboratory, Upton, New York 11973, United States;* ⓞ orcid.org/0000-0002-5451-1207; Email: anatoly.frenkel@stonybrook.edu

Authors

Junying Li − *Department of Materials Science and Chemical Engineering, Stony Brook University, Stony Brook, New York 11794, United States*

Peipei Huang − *Department of Chemistry, University of New Hampshire, Durham, New Hampshire 03857, United States*

Facheng Guo − *Department of Chemistry, Yale University, New Haven, Connecticut 06520, United States*

Jiahao Huang − *Department of Materials Science and Chemical Engineering, Stony Brook University, Stony Brook, New York 11794, United States*

Shuting Xiang − *Department of Materials Science and Chemical Engineering, Stony Brook University, Stony Brook, New York 11794, United States*

Ke Yang − *Department of Chemistry, Yale University, New Haven, Connecticut 06520, United States;* ⓞ orcid.org/0000-0003-0028-2717

N. Aaron Deskins − *Department of Chemical Engineering, Worcester Polytechnic Institute, Worcester, Massachusetts 01609, United States;* ⓞ orcid.org/0000-0002-0041-7960

Victor S. Batista − *Department of Chemistry, Yale University, New Haven, Connecticut 06520, United States;* ⓞ orcid.org/0000-0002-3262-1237

Complete contact information is available at:
https://pubs.acs.org/10.1021/acs.jpcc.2c08587

Notes

The authors declare no competing financial interest.

■ ACKNOWLEDGMENTS

■ REFERENCES

(1) Usman, M.; Humayun, M.; Garba, M. D.; Ullah, L.; Zeb, Z.; Helal, A.; Suliman, M. H.; Alfaifi, B. Y.; Iqbal, N.; Abdinejad, M.; Tahir, A. A.; Ullah, H. Electrochemical reduction of CO_2: a review of cobalt based catalysts for carbon dioxide conversion to fuels. *Nanomaterials* **2021**, *11*, 2029.

(2) Doney, S. C.; Fabry, V. J.; Feely, R. A.; Kleypas, J. A. Ocean acidification: the other CO_2 problem. *Annu. Rev. Mar. Sci.* **2009**, *1*, 169−192.

(3) Appel, A. M.; Bercaw, J. E.; Bocarsly, A. B.; Dobbek, H.; DuBois, D. L.; Dupuis, M.; Ferry, J. G.; Fujita, E.; Hille, R.; Kenis, P. J.;

Kerfeld, C. A.; Morris, R. H.; Peden, C. H. F.; Portis, A. R.; Ragsdale, S. W.; Rauchfuss, T. B.; Reek, J. N. H.; Seefeldt, L. C.; Thauer, R. K.; Waldrop, G. L. Frontiers, opportunities, and challenges in biochemical and chemical catalysis of CO_2 fixation. *Chem. Rev.* **2013**, *113*, 6621−6658.

(4) Draper, A. M.; Weissburg, M. J. Impacts of global warming and elevated CO_2 on sensory behavior in predator-prey interactions: a review and synthesis. *Front. Ecol. Evol.* **2019**, *7*, 72.

(5) Mikkelsen, M.; Jørgensen, M.; Krebs, F. C. The teraton challenge. A review of fixation and transformation of carbon dioxide. *Energy Environ. Sci.* **2010**, *3*, 43−81.

(6) Kumar, B.; Llorente, M.; Froehlich, J.; Dang, T.; Sathrum, A.; Kubiak, C. P. Photochemical and Photoelectrochemical Reduction of CO_2. *Annu. Rev. Phys. Chem.* **2012**, *63*, 541−569.

(7) van der Giesen, C.; Kleijn, R.; Kramer, G. J. Energy and Climate Impacts of Producing Synthetic Hydrocarbon Fuels from CO_2. *Environ. Sci. Technol.* **2014**, *48*, 7111−7121.

(8) White, J. L.; Baruch, M. F.; Pander, J. E.; Hu, Y.; Fortmeyer, I. C.; Park, J. E.; Zhang, T.; Liao, K.; Gu, J.; Yan, Y.; et al. Light-Driven Heterogeneous Reduction of Carbon Dioxide: Photocatalysts and Photoelectrodes. *Chem. Rev.* **2015**, *115*, 12888−12935.

(9) Benson, E. E.; Kubiak, C. P.; Sathrum, A. J.; Smieja, J. M. Electrocatalytic and homogeneous approaches to conversion of CO_2 to liquid fuels. *Chem. Soc. Rev.* **2009**, *38*, 89−99.

(10) Morris, A. J.; Meyer, G. J.; Fujita, E. Molecular Approaches to the Photocatalytic Reduction of Carbon Dioxide for Solar Fuels. *Acc. Chem. Res.* **2009**, *42*, 1983−1994.

(11) Koike, K.; Naito, S.; Sato, S.; Tamaki, Y.; Ishitani, O. Architecture of supramolecular metal complexes for photocatalytic CO_2 reduction. *J. Photochem. Photobiol., A* **2009**, *207*, 109−114.

(12) Wang, S.; Lin, J.; Wang, X. Semiconductor-redox catalysis promoted by metal-organic frameworks for CO_2 reduction. *Phys. Chem. Chem. Phys.* **2014**, *16*, 14656−14660.

(13) Tamaki, Y.; Ishitani, O. Supramolecular Photocatalysts for the Reduction of CO_2. *ACS Catal.* **2017**, *7*, 3394−3409.

(14) Wang, L.; Chen, W.; Zhang, D.; Du, Y.; Amal, R.; Qiao, S.; Wu, J.; Yin, Z. Surface strategies for catalytic CO_2 reduction: from two-dimensional materials to nanoclusters to single atoms. *Chem. Soc. Rev.* **2019**, *48*, 5310−5349.

(15) Kumar, P.; Joshi, C.; Labhsetwar, N.; Boukherroub, R.; Jain, S. L. A novel Ru/TiO_2 hybrid nanocomposite catalyzed photoreduction of CO_2 to methanol under visible light. *Nanoscale* **2015**, *7*, 15258−15267.

(16) Liras, M.; Barawi, M.; de la Pena O'Shea, V. A. Hybrid materials based on conjugated polymers and inorganic semiconductors as photocatalysts: from environmental to energy applications. *Chem. Soc. Rev.* **2019**, *48*, 5454−5487.

(17) He, J.; Janaky, C. Recent Advances in Solar-Driven Carbon Dioxide Conversion: Expectations versus Reality. *ACS Energy Lett.* **2020**, *5*, 1996−2014.

(18) Louis, M. E.; Fenton, T. G.; Rondeau, J.; Jin, T.; Li, G. Solar CO_2 Reduction Using Surface-Immobilized Molecular Catalysts. *Comments Inorg. Chem.* **2016**, *36*, 38−60.

(19) Wen, F.; Li, C. Hybrid Artificial Photosynthetic Systems Comprising Semiconductors as Light Harvesters and Biomimetic Complexes as Molecular Cocatalysts. *Acc. Chem. Res.* **2013**, *46*, 2355−2364.

(20) Sato, S.; Arai, T.; Morikawa, T. Toward Solar-Driven Photocatalytic CO_2 Reduction Using Water as an Electron Donor. *Inorg. Chem.* **2015**, *54*, 5105−5113.

(21) Windle, C. D.; Reisner, E. Heterogenised Molecular Catalysts for the Reduction of CO_2 to Fuels. *Chimia* **2015**, *69*, 435−441.

(22) Kuriki, R.; Sekizawa, K.; Ishitani, O.; Maeda, K. Visible-light-driven CO_2 reduction with carbon nitride: enhancing the activity of ruthenium catalysts. *Angew. Chem., Int. Ed.* **2015**, *54*, 2406−2409.

(23) Dalle, K. E.; Warnan, J.; Leung, J. J.; Reuillard, B.; Karmel, I. S.; Reisner, E. Electro-and solar-driven fuel synthesis with first row transition metal complexes. *Chem. Rev.* **2019**, *119*, 2752−2875.

(24) Pan, Y.; Lin, R.; Chen, Y.; Liu, S.; Zhu, W.; Cao, X.; Chen, W.; Wu, K.; Cheong, W.-C.; Wang, Y.; Zheng, L.; Luo, J.; Lin, Y.; Liu, Y.; Liu, C.; Li, J.; Lu, Q.; Chen, X.; Wang, D.; Peng, Q.; Chen, C.; Li, Y. Design of single-atom Co−N5 catalytic site: a robust electrocatalyst for CO_2 reduction with nearly 100% CO selectivity and remarkable stability. *J. Am. Chem. Soc.* **2018**, *140*, 4218−4221.

(25) Kaiser, S. K.; Chen, Z.; Faust Akl, D.; Mitchell, S.; Pérez-Ramírez, J. Single-atom catalysts across the periodic table. *Chem. Rev.* **2020**, *120*, 11703−11809.

(26) Wang, X.; Chen, Z.; Zhao, X.; Yao, T.; Chen, W.; You, R.; Zhao, C.; Wu, G.; Wang, J.; Huang, W.; Yang, J.; Hong, X.; Wei, S.; Wu, Y.; Li, Y. Regulation of coordination number over single Co sites: triggering the efficient electroreduction of CO_2. *Angew. Chem., Int. Ed.* **2018**, *57*, 1944−1948.

(27) Di, J.; Chen, C.; Yang, S.-Z.; Chen, S.; Duan, M.; Xiong, J.; Zhu, C.; Long, R.; Hao, W.; Chi, Z. Isolated single atom cobalt in Bi_3O_4Br atomic layers to trigger efficient CO_2 photoreduction. *Nat. Commun.* **2019**, *10*, 2840.

(28) Chu, C.; Zhu, Q.; Pan, Z.; Gupta, S.; Huang, D.; Du, Y.; Weon, S.; Wu, Y.; Muhich, C.; Stavitski, E. Spatially separating redox centers on 2D carbon nitride with cobalt single atom for photocatalytic H_2O_2 production. *Proc. Natl. Acad. Sci. U. S. A.* **2020**, *117*, 6376−6382.

(29) Roy, S.; Reisner, E. Visible-Light-Driven CO_2 Reduction by Mesoporous Carbon Nitride Modified with Polymeric Cobalt Phthalocyanine. *Angew. Chem., Int. Ed.* **2019**, *58*, 12180−12184.

(30) Shang, B.; Zhao, F.; Choi, C.; Jia, X.; Pauly, M.; Wu, Y.; Tao, Z.; Zhong, Y.; Harmon, N.; Maggard, P. A.; Lian, T.; Hazari, N.; Wang, H. Monolayer Molecular Functionalization Enabled by Acid−Base Interaction for High-Performance Photochemical CO_2 Reduction. *ACS Energy Lett.* **2022**, *7*, 2265−2272.

(31) Ma, B.; Chen, G.; Fave, C.; Chen, L.; Kuriki, R.; Maeda, K.; Ishitani, O.; Lau, T.-C.; Bonin, J.; Robert, M. Efficient visible-light-driven CO_2 reduction by a cobalt molecular catalyst covalently linked to mesoporous carbon nitride. *J. Am. Chem. Soc.* **2020**, *142*, 6188−6195.

(32) Matsuoka, S.; Yamamoto, K.; Ogata, T.; Kusaba, M.; Nakashima, N.; Fujita, E.; Yanagida, S. Efficient and selective electron mediation of cobalt complexes with cyclam and related macrocycles in the p-terphenyl-catalyzed photoreduction of carbon dioxide. *J. Am. Chem. Soc.* **1993**, *115*, 601−609.

(33) Liu, C.; Jin, T.; Louis, M. E.; Pantovich, S. A.; Skraba-Joiner, S. L.; Rajh, T.; Li, G. Molecular deposition of a macrocyclic cobalt catalyst on TiO_2 nanoparticles. *J. Mol. Catal. A: Chem.* **2016**, *423*, 293−299.

(34) Jin, T.; Liu, C.; Li, G. Photocatalytic CO_2 reduction using a molecular cobalt complex deposited on TiO_2 nanoparticles. *Chem. Commun.* **2014**, *50*, 6221−6224.

(35) Huang, P.; Pantovich, S. A.; Okolie, N. O.; Deskins, N. A.; Li, G. Hybrid Carbon Dioxide Reduction Photocatalysts Consisting of Macrocyclic Cobalt (III) Complexes Deposited on Semiconductor Surfaces. *ChemPhotoChem* **2020**, *4*, 420−426.

(36) Xiang, S.; Huang, P.; Li, J.; Liu, Y.; Marcella, N.; Routh, P. K.; Li, G.; Frenkel, A. I. Solving the structure of "single-atom" catalysts using machine learning−assisted XANES analysis. *Phys. Chem. Chem. Phys.* **2022**, *24*, 5116−5124.

(37) Huang, P.; Huang, J.; Li, J.; Zhang, L.; He, J.; Caputo, C. A.; Frenkel, A. I.; Li, G. Effect of Carbon Doping on CO_2-Reduction Activity of Single Cobalt Sites in Graphitic Carbon Nitride. *ChemNanoMat* **2021**, *7*, 1051−1056.

(38) Chen, Z.; Mitchell, S.; Vorobyeva, E.; Leary, R. K.; Hauert, R.; Furnival, T.; Ramasse, Q. M.; Thomas, J. M.; Midgley, P. A.; Dontsova, D.; Antonietti, M.; Pogodin, S.; López, N.; Pérez-Ramírez, J. Stabilization of single metal atoms on graphitic carbon nitride. *Adv. Funct. Mater.* **2017**, *27*, No. 1605785.

(39) Huang, P.; Huang, J.; Pantovich, S. A.; Carl, A. D.; Fenton, T. G.; Caputo, C. A.; Grimm, R. L.; Frenkel, A. I.; Li, G. Selective CO_2 reduction catalyzed by single cobalt sites on carbon nitride under visible-light irradiation. *J. Am. Chem. Soc.* **2018**, *140*, 16042−16047.

(40) Huang, P.; Huang, J.; Li, J.; Pham, T. D.; Zhang, L.; He, J.; Brudvig, G. W.; Deskins, N. A.; Frenkel, A. I.; Li, G. Revealing the Structure of Single Cobalt Sites in Carbon Nitride for Photocatalytic CO_2 Reduction. *J. Phys. Chem. C* **2022**, *126*, 8596−8604.

(41) Kottwitz, M.; Li, Y.; Wang, H.; Frenkel, A. I.; Nuzzo, R. G. Single atom catalysts: a review of characterization methods. *Chem. Methods* **2021**, *1*, 278−294.

(42) Zitolo, A.; Goellner, V.; Armel, V.; Sougrati, M.-T.; Mineva, T.; Stievano, L.; Fonda, E.; Jaouen, F. Identification of catalytic sites for oxygen reduction in iron-and nitrogen-doped graphene materials. *Nat. Mater.* **2015**, *14*, 937−942.

(43) Li, Y.; Frenkel, A. I. Deciphering the local environment of single-atom catalysts with X-ray absorption spectroscopy. *Acc. Chem. Res.* **2021**, *54*, 2660−2669.

(44) Wang, H.; Kottwitz, M.; Rui, N.; Senanayake, S. D.; Marinkovic, N.; Li, Y.; Nuzzo, R. G.; Frenkel, A. I. Aliovalent doping of CeO_2 improves the stability of atomically dispersed Pt. *ACS Appl. Mater. Interfaces* **2021**, *13*, 52736−52742.

(45) Kottwitz, M.; Li, Y.; Palomino, R. M.; Liu, Z.; Wang, G.; Wu, Q.; Huang, J.; Timoshenko, J.; Senanayake, S. D.; Balasubramanian, M.; Lu, D.; Nuzzo, R. G.; Frenkel, A. I. Local structure and electronic state of atomically dispersed Pt supported on nanosized CeO_2. *ACS Catal.* **2019**, *9*, 8738−8748.

(46) Rockenberger, J.; Tröger, L.; Kornowski, A.; Vossmeyer, T.; Eychmüller, A.; Feldhaus, J.; Weller, H. EXAFS studies on the size dependence of structural and dynamic properties of CdS nanoparticles. *J. Phys. Chem. B* **1997**, *101*, 2691−2701.

(47) Timoshenko, J.; Duan, Z.; Henkelman, G.; Crooks, R.; Frenkel, A. Solving the structure and dynamics of metal nanoparticles by combining X-ray absorption fine structure spectroscopy and atomistic structure simulations. *Annu. Rev. Anal. Chem.* **2019**, *12*, 501.

(48) Timoshenko, J.; Frenkel, A. I. Probing structural relaxation in nanosized catalysts by combining EXAFS and reverse Monte Carlo methods. *Catal. Today* **2017**, *280*, 274−282.

(49) Rehr, J.; Albers, R.; Zabinsky, S. High-order multiple-scattering calculations of X-ray-absorption fine structure. *Phys. Rev. Lett.* **1992**, *69*, 3397.

(50) Dalba, G.; Fornasini, P.; Grisenti, R.; Rocca, F. X-ray absorption fine structure: characterization of thermal and structural disorder in non-crystalline solids. *J. Non-Cryst. Solids* **2004**, *345−346*, 7−15.

(51) Ankudinov, A. L.; Ravel, B.; Rehr, J.; Conradson, S. Real-space multiple-scattering calculation and interpretation of x-ray-absorption near-edge structure. *Phys. Rev. B* **1998**, *58*, 7565.

(52) Li, J.; Li, Y.; Routh, P. K.; Makagon, E.; Lubomirsky, I.; Frenkel, A. I. Comparative analysis of XANES and EXAFS for local structural characterization of disordered metal oxides. *J. Synchrotron Radiat.* **2021**, *28*, 1511.

(53) Liu, J. Catalysis by supported single metal atoms. *ACS Catal.* **2017**, *7*, 34−59.

(54) Ravel, B.; Newville, M. ATHENA, ARTEMIS, HEPHAESTUS: data analysis for X-ray absorption spectroscopy using IFEFFIT. *J. Synchrotron Radiat.* **2005**, *12*, 537−541.

(55) Rehr, J. J.; Kas, J. J.; Vila, F. D.; Prange, M. P.; Jorissen, K. Parameter-free calculations of X-ray spectra with FEFF9. *Phys. Chem. Chem. Phys.* **2010**, *12*, 5503−5513.

(56) Kresse, G.; Furthmüller, J. Efficiency of ab-initio total energy calculations for metals and semiconductors using a plane-wave basis set. *Comput. Mater. Sci.* **1996**, *6*, 15−50.

(57) Kresse, G.; Furthmüller, J. Efficient iterative schemes for ab initio total-energy calculations using a plane-wave basis set. *Phys. Rev. B* **1996**, *54*, 11169.

(58) Kresse, G.; Hafner, J. Ab initio molecular dynamics for liquid metals. *Phys. Rev. B* **1993**, *47*, 558.

(59) Kresse, G.; Hafner, J. Ab initio molecular-dynamics simulation of the liquid-metal−amorphous-semiconductor transition in germanium. *Phys. Rev. B* **1994**, *49*, 14251.

(60) Perdew, J. P.; Burke, K.; Ernzerhof, M. Generalized gradient approximation made simple. *Phys. Rev. Lett.* **1996**, *77*, 3865.

(61) Blöchl, P. E. Projector augmented-wave method. *Phys. Rev. B* **1994**, *50*, 17953.

(62) Kresse, G.; Joubert, D. From ultrasoft pseudopotentials to the projector augmented-wave method. *Phys. Rev. B* **1999**, *59*, 1758.

(63) Grimme, S.; Antony, J.; Ehrlich, S.; Krieg, H. A consistent and accurate ab initio parametrization of density functional dispersion correction (DFT-D) for the 94 elements H-Pu. *J. Chem. Phys.* **2010**, *132*, 154104.

(64) Johnson, E. R.; Becke, A. D. A post-Hartree-Fock model of intermolecular interactions: Inclusion of higher-order corrections. *J. Chem. Phys.* **2006**, *124*, 174104.

(65) Monkhorst, H. J.; Pack, J. D. Special points for Brillouin-zone integrations. *Phys. Rev. B* **1976**, *13*, 5188.

(66) Funston, A. M.; Mcfadyen, W. D.; Tregloan, P. A. The synthesis and crystal structures of two cobalt (III) complexes containing the ligand 1, 4, 8, 11-tetraazacyclotetradecane. *Aust. J. Chem.* **2002**, *55*, 535−538.

(67) Oba, Y.; Mochida, T. Thermal properties and crystal structures of cobalt (III)−cyclam complexes with the bis (trifluoromethane-sulfonyl) amide anion (cyclam= 1, 4, 8, 11-tetraazacyclotetradecane). *Polyhedron* **2015**, *99*, 275−279.

(68) Wang, W.-F.; Zhang, Y.-K.; Feng, L.-F.; Li, H.-R.; He, L.-N. In-plane benzene incorporated g-C_3N_4 microtubes: Enhanced visible light harvesting and carrier transportation for photocatalytic CO_2 reduction. *Fuel* **2022**, *326*, No. 125073.

(69) Liu, Y.; Marcella, N.; Timoshenko, J.; Halder, A.; Yang, B.; Kolipaka, L.; Pellin, M. J.; Seifert, S.; Vajda, S.; Liu, P.; et al. Mapping XANES spectra on structural descriptors of copper oxide clusters using supervised machine learning. *J. Chem. Phys.* **2019**, *151*, 164201.

(70) Liu, Y.; Halder, A.; Seifert, S.; Marcella, N.; Vajda, S.; Frenkel, A. I. Probing active sites in CuxPdy cluster catalysts by machine-learning-assisted X-ray absorption spectroscopy. *ACS Appl. Mater. Interfaces* **2021**, *13*, 53363−53374.

(71) Andrejevic, N.; Andrejevic, J.; Bernevig, B. A.; Regnault, N.; Han, F.; Fabbris, G.; Nguyen, T.; Drucker, N. C.; Rycroft, C. H.; Li, M., Machine Learning Spectral Indicators of Topology. In *Machine Learning-Augmented Spectroscopies for Intelligent Materials Design*; Springer International Publishing: Cham, 2022; pp 79−93.